

Localized magnetic states in biased bilayer and trilayer graphene

This article has been downloaded from IOPscience. Please scroll down to see the full text article.

2009 J. Phys.: Condens. Matter 21 182002

(<http://iopscience.iop.org/0953-8984/21/18/182002>)

[View the table of contents for this issue](#), or go to the [journal homepage](#) for more

Download details:

IP Address: 129.252.86.83

The article was downloaded on 29/05/2010 at 19:29

Please note that [terms and conditions apply](#).

FAST TRACK COMMUNICATION

Localized magnetic states in biased bilayer and trilayer graphene

Kai-He Ding¹, Zhen-Gang Zhu² and Jamal Berakdar²

¹ Department of Physics and Electronic Science, Changsha University of Science and Technology, Changsha 410076, People's Republic of China

² Institut für Physik Martin-Luther-Universität Halle-Wittenberg, Nanotechnikum-Weinberg, Heinrich-Damerow-Strasse 4 D-06120 Halle (Saale), Germany

Received 23 February 2009

Published 31 March 2009

Online at stacks.iop.org/JPhysCM/21/182002

Abstract

We study the localized magnetic states of an impurity in biased bilayer and trilayer graphene. It is found that the magnetic boundary for bilayer and trilayer graphene shows mixed features of Dirac and conventional fermions. For zero gate bias, as the impurity energy approaches the Dirac point, the impurity magnetization region diminishes for bilayer and trilayer graphene. When a gate bias is applied, the dependence of impurity magnetic states on the impurity energy exhibits a different behavior for bilayer and trilayer graphene due to the opening of a gap between the valence and the conduction band in the bilayer graphene with an applied gate bias. The magnetic moment and the corresponding magnetic transition of the impurity in bilayer graphene are also investigated.

1. Introduction

The intense research currently devoted to graphene, a two-dimensional carbon honeycomb lattice, has uncovered a wealth of fascinating properties such as the anomalous quantized Hall effect, the absence of weak localization and the existence of minimal conductivity [1–5]. Graphene has a high mobility and its carrier density is controllable by an applied gate voltage [2] and a spin-orbit interaction [6–10].

Graphene structures have been the focus of much interest [12–20, 26]. In particular, adatoms may be positioned on graphene by current nanotechnology [21], rendering the study and manipulation of local electronic properties. *Ab initio* calculations for transition metal adatoms [22] show a tendency to the formation of local magnetic moments. Recently Uchoa *et al* [23] examined the condition for the emergence of localized magnetic moments on adatoms with inner shell electrons on a single-layer graphene. It is found that the impurity magnetization boundary exhibits anomalous characteristics. In contrast to the case of an impurity in an ordinary metal, the impurity can magnetize for any small charging energy due to the low density of state (DOS) at the Dirac point. On the other hand, detailed experimental studies [26] on multi-layer graphene showed

a marked modification of the electronic structure with the number of layers. Hence, we expect [11] a qualitative difference in the magnetic properties of the adatoms on multi-layer graphene; an issue which we address here by inspecting the localized magnetic state of an impurity in a biased bilayer and trilayer graphene. We find that the size of the magnetic region decreases rapidly compared with that in monolayer graphene, the impurity can magnetize even when the energy of the doubly occupied state is below the Fermi level. The impurity magnetization region is asymmetric due to the special nature of the quasiparticles having mixed features of Dirac and conventional fermions. When a gate bias is applied, the dependence of the impurity magnetic states on the impurity energy for a bilayer graphene exhibits a different behavior from that for a trilayer graphene due to the opening of a gate-induced gap between the valence and the conduction band in the bilayer graphene. Calculating the occupation of the impurity level and the susceptibility in the bilayer graphene we show that the magnetic moment decreases with increasing the inter-layer coupling.

2. Bilayer graphene

Figure 1 shows the lattice structure of the bilayer graphene with the adatom. The inter-layer stacking is assumed to be the

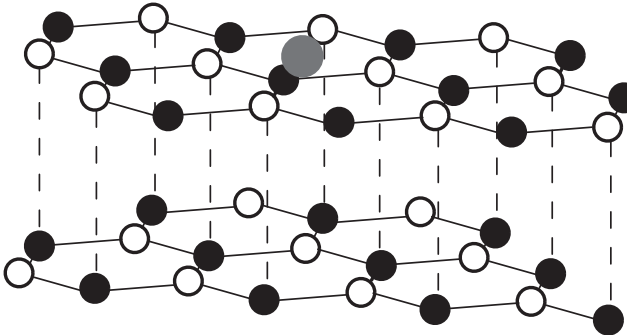


Figure 1. Schematic diagram of the lattice structure of the bilayer graphene with an impurity atom.

Bernal order where the top layer has its A sublattice atop the sublattice B of the bottom layer. The bias voltage V is applied across the layers. The system Hamiltonian

$$H = H_{\text{TB}} + H_i + H_f \quad (1)$$

contains the graphene bilayer term H_{TB} , which in a tight-binding approximation reads

$$H_{\text{TB}} = \sum_{l=1}^2 H_l + H_T + H_V, \quad (2)$$

with

$$H_l = -t \sum_{\langle i, j \rangle \sigma} [a_{l\sigma}^\dagger(\mathbf{R}_i) b_{l\sigma}(\mathbf{R}_j) + b_{l\sigma}^\dagger(\mathbf{R}_j) a_{l\sigma}(\mathbf{R}_i)], \quad (3)$$

$$H_T = -t_p \sum_{i, \sigma} [a_{1\sigma}^\dagger(\mathbf{R}_i) b_{2\sigma}(\mathbf{R}_i) + b_{2\sigma}^\dagger(\mathbf{R}_i) a_{1\sigma}(\mathbf{R}_i)], \quad (4)$$

$$H_V = \frac{V}{2} \sum_{i\sigma} [a_{1\sigma}^\dagger(\mathbf{R}_i) a_{1\sigma}(\mathbf{R}_i) + b_{1\sigma}^\dagger(\mathbf{R}_i) b_{1\sigma}(\mathbf{R}_i) - a_{2\sigma}^\dagger(\mathbf{R}_i) a_{2\sigma}(\mathbf{R}_i) - b_{2\sigma}^\dagger(\mathbf{R}_i) b_{2\sigma}(\mathbf{R}_i)]. \quad (5)$$

The operator $a_{l\sigma}(\mathbf{R}_i)$ ($b_{l\sigma}(\mathbf{R}_i)$) annihilates a state with a spin σ at the position \mathbf{R}_i on the sublattice A(B) of the l plane. t is the nearest neighbour in-plane hopping energy, t_p is the inter-layer hopping energy. For the hybridization with the localized impurity states we write

$$H_i = V_f \sum_{\sigma} [f_{\sigma}^\dagger b_{1\sigma}(0) + b_{1\sigma}^\dagger(0) f_{\sigma}], \quad (6)$$

where $f_{\sigma}(f_{\sigma}^\dagger)$ is the annihilation (creation) operator of a state with a spin σ at the impurity, and V_f is the hybridization strength. In the momentum space we have

$$H_l = -t \sum_{\mathbf{k}\sigma} [\phi(\mathbf{k}) a_{l\mathbf{k}\sigma}^\dagger b_{l\mathbf{k}\sigma} + \phi^*(\mathbf{k}) b_{l\mathbf{k}\sigma}^\dagger a_{l\mathbf{k}\sigma}], \quad (7)$$

$$H_T = t_p \sum_{\mathbf{k}, \sigma} [a_{1\mathbf{k}\sigma}^\dagger b_{2\mathbf{k}\sigma} + b_{2\mathbf{k}\sigma}^\dagger a_{1\mathbf{k}\sigma}], \quad (8)$$

$$H_V = \frac{V}{2} \sum_{\mathbf{k}\sigma} [a_{1\mathbf{k}\sigma}^\dagger a_{1\mathbf{k}\sigma} + b_{1\mathbf{k}\sigma}^\dagger b_{1\mathbf{k}\sigma} - a_{2\mathbf{k}\sigma}^\dagger a_{2\mathbf{k}\sigma} - b_{2\mathbf{k}\sigma}^\dagger b_{2\mathbf{k}\sigma}], \quad (9)$$

$$H_i = \frac{V_f}{\sqrt{N}} \sum_{\mathbf{k}\sigma} (f_{\sigma}^\dagger b_{1\mathbf{k}\sigma} + b_{1\mathbf{k}\sigma}^\dagger f_{\sigma}), \quad (10)$$

where $\phi(\mathbf{q}) = -t \sum_{i=1}^3 e^{i\mathbf{q} \cdot \delta_i}$ with $\delta_1 = \frac{a}{2}(1, \sqrt{3}, 0)$, $\delta_2 = \frac{a}{2}(1, -\sqrt{3}, 0)$, $\delta_3 = a(1, 0, 0)$ (here a is the lattice spacing), and N is the number of sites on sublattice B of plane 1. Diagonalizing H_{TB} we find the spectrum

$$E_{\pm\pm}(\mathbf{k}) = \pm \sqrt{\epsilon_k^2 + \frac{t_p^2}{2} + \frac{V^2}{4} \pm \sqrt{\frac{t_p^4}{4} + (t_p^2 + V^2)\epsilon_k^2}}, \quad (11)$$

where $\epsilon_k = \pm |\phi(\mathbf{k})|$ is linearizable around the \mathbf{K} points of the Brillouin zone by $\epsilon_k = \pm v_F |\mathbf{k}|$ where $v_F = 3ta/2$ is the Fermi velocity. The impurity is described by the Hamiltonian H_f with

$$H_f = \sum_{\sigma} \varepsilon_0 f_{\sigma}^\dagger f_{\sigma} + U n_{\uparrow} n_{\downarrow}, \quad (12)$$

where $n_{\sigma} = f_{\sigma}^\dagger f_{\sigma}$ is the occupation number operator, ε_0 is the single electron energy at the impurity. The Coulomb interaction is included as a finite Anderson term U . For simplicity, we adopt a mean field approximation to the electronic correlations at the impurity, $U n_{\uparrow} n_{\downarrow} \simeq U \sum_{\sigma} \langle n_{\sigma} \rangle f_{\sigma}^\dagger f_{\sigma} - U \langle n_{\uparrow} \rangle \langle n_{\downarrow} \rangle$. The impurity Hamiltonian is rewritten as $H_f = \sum_{\sigma} \varepsilon_{\sigma} f_{\sigma}^\dagger f_{\sigma}$ with $\varepsilon_{\sigma} = \varepsilon_0 + U \langle n_{\sigma} \rangle$. To investigate the localized magnetic states, we calculate the occupation number of the electrons of a given spin σ at the impurity. At low temperatures all the states below the Fermi level μ are completely occupied and the occupation of the impurity is determined by

$$\langle n_{\sigma} \rangle = \int_{-\infty}^{\mu} d\omega \rho_f^{\sigma}(\omega), \quad (13)$$

where $\rho_f^{\sigma}(\omega)$ is the DOS at the impurity level. We infer this from the retarded Green's function

$$G_f^{r, \sigma \sigma'}(t - t') = -i\theta(t - t') \langle \{f_{\sigma}(t), f_{\sigma'}^\dagger(t')\} \rangle. \quad (14)$$

By the standard equation of motion, we can derive ($\eta \rightarrow 0^+$)

$$G_f^{r, \sigma \sigma'}(\omega) = \frac{\delta_{\sigma \sigma'}}{\omega - \varepsilon_{\sigma} - \Sigma_f^r(\omega) + i\eta}, \quad (15)$$

where

$$\Sigma_f^r(\omega) = \frac{V_f^2}{N} \sum_{\mathbf{k}} \frac{-(\omega - \frac{V}{2}) v_F^2 |\mathbf{k}|^2 + (\omega - \frac{V}{2})(\omega + \frac{V}{2})^2 - t_p^2(\omega + \frac{V}{2})}{v_F^4 |\mathbf{k}|^4 - 2(\omega^2 + \frac{V^2}{4}) v_F^2 |\mathbf{k}|^2 + (\omega^2 - \frac{V^2}{2})^2 - t_p^2(\omega^2 - \frac{V^2}{4})}. \quad (16)$$

Introducing a high-energy cutoff D of the graphene bandwidth, we obtain for $\omega^2 \geq \frac{1}{4} \frac{t_p^2 V^2}{t_p^2 + V^2}$,

$$\Sigma_f^r(\omega) = \frac{V_f^2}{D^2} \left\{ \frac{V\omega^2 - (V^2/2 + t_p^2)\omega - Vt_p^2/2}{\sqrt{4(V^2 + t_p^2)\omega^2 - t_p^2 V^2}} \right. \\ \times \ln \left| \frac{(D^2 - x_1)x_2}{(D^2 - x_2)x_1} \right| - \frac{\omega - V/2}{2} \\ \left. \times \ln \left| \frac{(D^2 - x_1)(D^2 - x_2)}{x_1 x_2} \right| \right\}$$

$$\begin{aligned}
& + i \frac{\pi V_f^2}{D^2} \left\{ \frac{V\omega^2 - (V^2/2 + t_p^2)\omega - Vt_p^2/2}{\sqrt{4(V^2 + t_p^2)\omega^2 - t_p^2V^2}} \right. \\
& \times \left[\operatorname{sgn} \left(\frac{dx_1}{d\omega} \right) \theta(0 < x_1 < D^2) \right. \\
& - \operatorname{sgn} \left(\frac{dx_2}{d\omega} \right) \theta(0 < x_2 < D^2) \\
& - \frac{\omega - V/2}{2} \left[\operatorname{sgn} \left(\frac{dx_1}{d\omega} \right) \theta(0 < x_1 < D^2) \right. \\
& \left. \left. + \operatorname{sgn} \left(\frac{dx_2}{d\omega} \right) \theta(0 < x_2 < D^2) \right] \right\}, \quad (17)
\end{aligned}$$

where $\theta(x)$ is the step function, and

$$x_{1,2} = \left(\omega^2 + \frac{V^2}{4} \right) \pm \frac{1}{2} \sqrt{4(V^2 + t_p^2)\omega^2 - t_p^2V^2}. \quad (18)$$

For $\omega^2 < \frac{1}{4} \frac{t_p^2 V^2}{t_p^2 + V^2}$,

$$\begin{aligned}
\Sigma_f^r(\omega) = & \frac{V_f^2}{D^2} \left[-\frac{\omega - V/2}{2} \right. \\
& \times \ln \left| \frac{D^4 - 2(\omega^2 + V^2/4)D^2 + (\omega^2 - V^2/2)^2 - t_p^2(\omega^2 - V^2/4)}{(\omega^2 - V^2/2)^2 - t_p^2(\omega^2 - V^2/4)} \right| \\
& + \frac{V\omega^2 - (V^2/2 + t_p^2)\omega - Vt_p^2/2}{\sqrt{t_p^2V^2/4 - (V^2 + t_p^2)\omega^2}} \\
& \times \left(\arctan \frac{D^2 - \omega^2 - V^2/4}{\sqrt{t_p^2V^2/4 - (V^2 + t_p^2)\omega^2}} \right. \\
& \left. + \arctan \frac{\omega^2 + V^2/4}{\sqrt{t_p^2V^2/4 - (V^2 + t_p^2)\omega^2}} \right). \quad (19)
\end{aligned}$$

The summation over \mathbf{k} in equation (16) is accurate for $\omega \ll D$ by ensuring the conservation of the total number of states in the Brillouin zone according to the Debye prescription. Substituting $\Sigma_f^r(\omega)$ into equation (15), the retarded Green's function $G_f^{r,\sigma\sigma}(\omega)$ can be obtained. Note, the determination of $\langle n_\sigma \rangle$ in equation (13) entails a self-consistent calculation of DOS at the impurity level via the relation $\rho_f^\sigma(\omega) = -\frac{1}{\pi} \operatorname{Im} G_f^{r,\sigma\sigma}(\omega)$. When $t_p = V = 0$, our present results reduce to those of [23].

3. Trilayer graphene

The Hamiltonian for trilayer graphene contains a coupling of the B atom of the second layer to the A atom of the third layer according to the conventional Bernal-type stacking order. Similar to the bilayer graphene case, we find for the impurity Green's function

$$G_f^{r,\sigma\sigma'}(\omega) = \frac{\delta_{\sigma\sigma'}}{\omega - \epsilon_\sigma - \Sigma^r + i\eta}, \quad (20)$$

where

$$\Sigma^r = -\frac{V_f^2}{N} \sum_{\mathbf{k}} \frac{A_1 v_F^4 |\mathbf{k}|^4 + B_1 v_F^2 |\mathbf{k}|^2 + C_1}{v_F^6 |\mathbf{k}|^6 + B_2 v_F^4 |\mathbf{k}|^4 + C_2 v_F^2 |\mathbf{k}|^2 + D_2} \quad (21)$$

with $A_1 = \omega - \frac{V}{2}$, $B_1 = t_p^2 \omega - (\omega - \frac{V}{2})[\omega^2 + (\omega + \frac{V}{2})^2]$, $C_1 = \omega^2(\omega - \frac{V}{2})(\omega + \frac{V}{2})^2 - 2t_p^2 \omega^2(\omega + \frac{V}{2})$, $B_2 = -3\omega^2 - \frac{V^2}{2}$, $C_2 = -2t_p^2 \omega^2 + 3\omega^4 + \frac{V^4}{16}$, $D_2 = -\omega^2(\omega^2 - \frac{V^2}{4})^2 + 2t_p^2 \omega^2(\omega^2 - \frac{V^2}{4})$. Performing the summation over \mathbf{k} in equation (21) as equation (16) we find for $\Delta = (2B_2^3 - 9B_2C_2 + 27D_2)^2 + 4(-B_2^2 + 3C_2)^3 \geq 0$ the result

$$\begin{aligned}
\Sigma^r = & -\frac{V_f^2}{D^2} \left\{ \left[A_1 + \frac{A_1(x_2 + x_3)x_1 + B_1x_1 - A_1x_2x_3 + C_1}{(x_2 - x_1)(x_3 - x_1)} \right. \right. \\
& \times \ln \left| \frac{D^2 - x_1}{x_1} \right| + \frac{A_1(x_2 + x_3) + B_1}{\sqrt{x_2x_3 - (x_2 + x_3)^2/4}} \\
& \times \left(\arctan \frac{D^2 - (x_2 + x_3)/2}{\sqrt{x_2x_3 - (x_2 + x_3)^2/4}} \right. \\
& \left. + \arctan \frac{(x_2 + x_3)/2}{\sqrt{x_2x_3 - (x_2 + x_3)^2/4}} \right) \\
& + \frac{A_1(x_2 + x_3)x_1 + B_1x_1 - A_1x_2x_3 + C_1}{(x_2 - x_1)(x_3 - x_1)} \\
& \times \left[\frac{-1}{2} \ln \frac{D^2 - (x_2 + x_3) + x_2x_3}{x_2x_3} \right. \\
& + \frac{(x_2 + x_3)/2 - x_1}{2\sqrt{x_2x_3 - (x_2 + x_3)^2/4}} \\
& \times \left(\arctan \frac{D^2 - (x_2 + x_3)/2}{\sqrt{x_2x_3 - (x_2 + x_3)^2/4}} \right. \\
& \left. + \arctan \frac{(x_2 + x_3)/2}{\sqrt{x_2x_3 - (x_2 + x_3)^2/4}} \right) \left. \right] \\
& - i \operatorname{sgn} \left(\frac{dx_1}{d\omega} \right) \theta(0 < x_1 < D^2) \frac{\pi V_f^2}{D^2} \\
& \times \left[A_1 + \frac{A_1(x_2 + x_3)x_1 + B_1x_1 - A_1x_2x_3 + C_1}{(x_2 - x_1)(x_3 - x_1)} \right], \quad (22)
\end{aligned}$$

where

$$\begin{aligned}
x_1 = & -\frac{B_2}{3} + \frac{1}{2^{1/3}} \frac{1}{3} \left\{ -2B_2^3 + 9B_2C_2 - 27D_2 \right. \\
& + \sqrt{(2B_2^3 - 9B_2C_2 + 27D_2)^2 + 4(-B_2^2 + 3C_2)^3} \left. \right\}^{\frac{1}{3}} \\
& + \frac{1}{2^{1/3}3} \left\{ -2B_2^3 + 9B_2C_2 - 27D_2 \right. \\
& - \sqrt{(2B_2^3 - 9B_2C_2 + 27D_2)^2 + 4(-B_2^2 + 3C_2)^3} \left. \right\}^{\frac{1}{3}}, \quad (23)
\end{aligned}$$

$$\begin{aligned}
x_{2,3} = & -\frac{B_2}{3} + \frac{-\frac{1}{2} - i\frac{\sqrt{3}}{2}}{3} \frac{1}{2^{1/3}} \left\{ -2B_2^3 + 9B_2C_2 - 27D_2 \right. \\
& \pm \sqrt{(2B_2^3 - 9B_2C_2 + 27D_2)^2 + 4(-B_2^2 + 3C_2)^3} \left. \right\}^{\frac{1}{3}} \\
& + \frac{-\frac{1}{2} + i\frac{\sqrt{3}}{2}}{3} \frac{1}{2^{1/3}} \left\{ -2B_2^3 + 9B_2C_2 - 27D_2 \right. \\
& \mp \sqrt{(2B_2^3 - 9B_2C_2 + 27D_2)^2 + 4(-B_2^2 + 3C_2)^3} \left. \right\}^{\frac{1}{3}}. \quad (24)
\end{aligned}$$

For $\Delta < 0$,

$$\begin{aligned}
\Sigma^r = & -\frac{V_f^2}{D^2} \left\{ \left[A_1 + \frac{[A_1(x_2 + x_3) + B_1]x_1 - A_1x_2x_3 + C_1}{(x_2 - x_1)(x_3 - x_1)} \right. \right. \\
& \times \ln \left| \frac{D^2 - x_1}{x_1} \right| - \left[\frac{A_1(x_2 + x_3) + B_1}{x_3 - x_2} \right. \\
& \left. \left. \right] \right\}
\end{aligned}$$

$$\begin{aligned}
& + \left[\frac{[A_1(x_2 + x_3) + B_1]x_1 - A_1x_2x_3 + C_1}{(x_2 - x_1)(x_3 - x_2)} \right] \ln \left| \frac{D^2 - x_2}{x_2} \right| \\
& + \left[\frac{A_1(x_2 + x_3) + B_1}{x_3 - x_2} \right] \\
& + \left[\frac{[A_1(x_2 + x_3) + B_1]x_1 - A_1x_2x_3 + C_1}{(x_2 - x_1)(x_3 - x_2)} \right. \\
& \left. - \frac{[A_1(x_2 + x_3) + B_1]x_1 - A_1x_2x_3 + C_1}{(x_2 - x_1)(x_3 - x_1)} \right] \\
& \times \ln \left| \frac{D^2 - x_3}{x_3} \right| \left\{ -i \frac{\pi V_f^2}{D^2} \left\{ \operatorname{sgn} \left(\frac{dx_1}{d\omega} \right) \theta(0 < x_1 < D^2) \right. \right. \\
& \times \left[A_1 + \frac{[A_1(x_2 + x_3) + B_1]x_1 - A_1x_2x_3 + C_1}{(x_2 - x_1)(x_3 - x_1)} \right] \\
& - \operatorname{sgn} \left(\frac{dx_2}{d\omega} \right) \theta(0 < x_2 < D^2) \left[\frac{A_1(x_2 + x_3) + B_1}{x_3 - x_2} \right. \\
& \left. + \frac{[A_1(x_2 + x_3) + B_1]x_1 - A_1x_2x_3 + C_1}{(x_2 - x_1)(x_3 - x_2)} \right] \\
& + \operatorname{sgn} \left(\frac{dx_3}{d\omega} \right) \theta(0 < x_3 < D^2) \left[\frac{A_1(x_2 + x_3) + B_1}{x_3 - x_2} \right. \\
& \left. + \frac{[A_1(x_2 + x_3) + B_1]x_1 - A_1x_2x_3 + C_1}{(x_2 - x_1)(x_3 - x_2)} \right. \\
& \left. - \frac{[A_1(x_2 + x_3) + B_1]x_1 - A_1x_2x_3 + C_1}{(x_2 - x_1)(x_3 - x_1)} \right] \left. \right\}, \quad (25)
\end{aligned}$$

where

$$x_1 = -\frac{B_2}{3} + \frac{2\sqrt{B_2^2 - 3C_2}}{3} \cos \left(\frac{\arccos T}{3} \right), \quad (26)$$

$$x_2 = -\frac{B_2}{3} + \frac{2\sqrt{B_2^2 - 3C_2}}{3} \cos \left(\frac{2\pi + \arccos T}{3} \right),$$

$$x_3 = -\frac{B_2}{3} + \frac{2\sqrt{B_2^2 - 3C_2}}{3} \cos \left(\frac{4\pi + \arccos T}{3} \right), \quad (27)$$

$$T = -\frac{2(B_2^2 - 3C_2)B_2 - 3(B_2C_2 - 9D_2)}{2(B_2^2 - 3C_2)^{\frac{3}{2}}}.$$

Substituting equations (22) and (25) in equation (20), we can derive self-consistently the occupation on the impurity for the case of a trilayer graphene.

4. Numerical analysis

From the occupation of the two spin channels on the impurity we conclude that a localized magnetic moment forms whenever $n_\uparrow \neq n_\downarrow$. For a detailed study, conventionally one introduces the dimensionless parameters

$$x = D\Gamma/U \quad \text{and} \quad y = (\mu - \varepsilon_0)/U$$

with $\Gamma = \pi V_f^2/D^2$. (28)

The transition curves from the magnetic to the non-magnetic behavior as a function of the parameters x and y for the different hybridization and inter-layer coupling in the bilayer graphene are shown in figure 2. For $t_p = V = 0$, our results reduce to those of [23]. The magnetic boundary exhibits

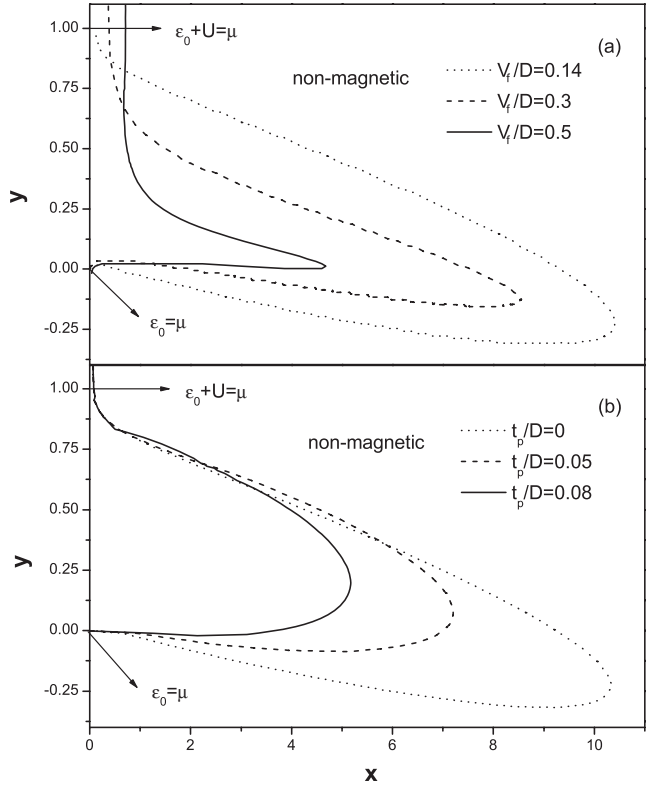


Figure 2. Regions of the magnetic and the non-magnetic phase for the bilayer graphene. The boundary line gives y as a function of x (defined in equation (28)) at $t_p/D = 0$ for the different V_f/D (a) and at $V_f/D = 0.14$ for different t_p/D (b). The other parameters are $\varepsilon_0/D = 0.029$ and $V/D = 0$.

an asymmetry around $y = 0.5$ and can even cross the line $y = 1$. The magnetic region shrinks in the x direction when the hybridization V_f is increased; for y close to 1 (cf equation (28)), the boundary line for magnetic transition shifts away from the y axis due to the increased influence of graphene on the impurity magnetization with enhanced hybridization. When the inter-layer coupling t_p is taken into account (see figure 2(b)), the size of the magnetic region diminishes rapidly, and for a large enough t_p , the magnetic boundary shrinks above the line $y = 0$. However, the magnetic boundary does not turn symmetric around $y = 0.5$ and the above magnetic boundary line crosses the line $y = 1$. The origin of this phenomena lies in the peculiar nature of the quasiparticles in the bilayer graphene; they exhibit features akin both to Dirac and to conventional fermions. The contribution of conventional fermions originates from the inter-layer coupling that supports a metallic bilayer graphene and results in effects as for a conventional metallic host on the magnetic properties of the impurity. For large inter-layer coupling we observe, therefore, magnetic boundaries similar to those for an impurity in an ordinary metal. Figure 3 shows for a bilayer graphene the boundary between magnetic and non-magnetic impurity states as a function of the parameters x and y (equation (28)) for different impurity energy levels ε_0 . For $V = 0$ the size of the magnetic region grows as ε_0 approaches the energy of the Dirac point. This behavior is reminiscent of the single layer of graphene [23], and originates

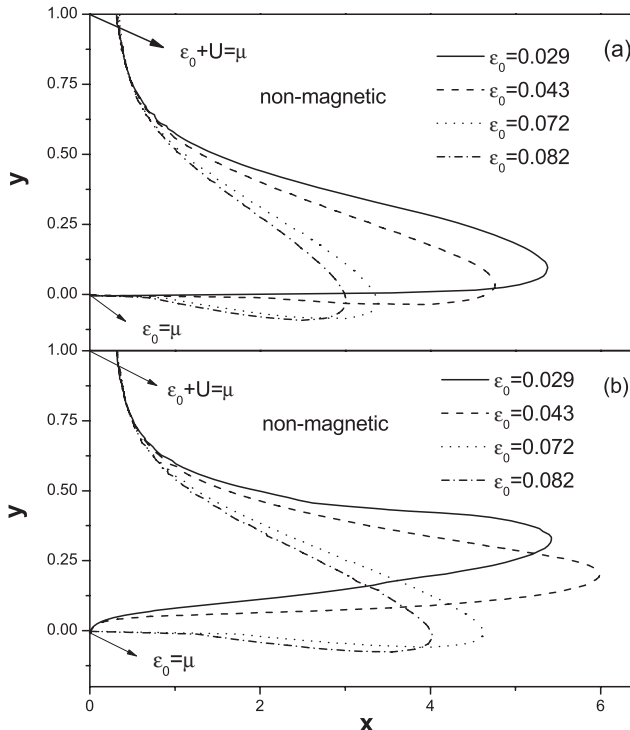


Figure 3. Regions of magnetic and non-magnetic phase for the bilayer graphene. The boundary line gives y as a function of x for the different ε_0/D at $V/D = 0$ (a) and at $V/D = 0.05$ (b), where $V_f/D = 0.3$ and $t_p/D = 0.05$.

from the suppression of the DOS around the impurity energy level. In contrast, for a nonzero gate bias, when ε_0 is close to the Dirac point from the positive energy side, the size of the region first increases to a maximum, then decreases with decreasing ε_0 , as shown in figure 3(b). The explanation for this phenomenon is as follows: the gate bias voltage gives rise to a finite electronic gap between the conduction and the valence band, and induces a large local DOS close to the gap edges [24]. In particular, the DOS may extend into the gap due to the influence of the impurity [25]. In this situation, the coupling between the bath and the impurity is enhanced inside the gap as compared with the zero bias case, leading thus to the non-monotonic dependence of the size of the region with ε_0 .

Figure 4 shows the magnetic transition curve as a function of the parameters x and y (equation (28)) for different ε_0 in the trilayer graphene. For $V = 0$, phenomena such as the asymmetry around the line $y = 0.5$ and the crossing of the line $y = 1$ in the magnetic boundary suggest the existence of Dirac fermions in the trilayer graphene. As ε_0 approaches the energy of the Dirac point, the magnetization region of the impurity grows due to the two almost-linear touching bands reminiscent of the bands in monolayer graphene [26]. It is interesting to note that for nonzero gate bias, the impurity magnetization region increases monotonously when ε_0 is close to the Dirac point, which is clearly different from that in the bilayer graphene. This behavior stems from the fact that the gate bias cannot destroy the particle-hole degeneracy in the trilayer graphene [26].

To investigate the localized magnetic moment of the impurity in the magnetic region and the magnetic transition

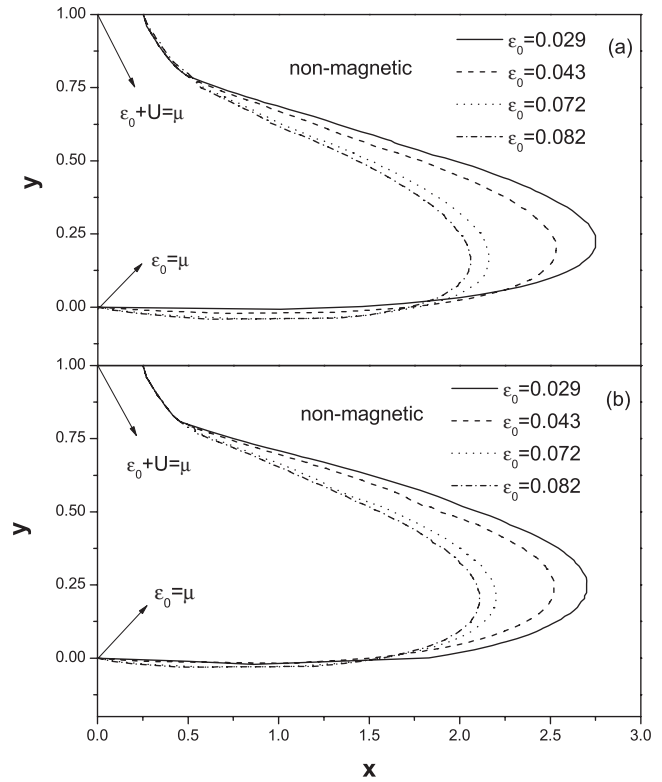


Figure 4. Regions of magnetic and non-magnetic phase for the trilayer graphene. The boundary line gives y as a function of x for the different ε_0/D at $V/D = 0$ (a) and at $V/D = 0.05$ (b), where $V_f/D = 0.2$ and $t_p/D = 0.05$.

we calculate the magnetic susceptibility. The energy of the impurity spin states in a magnetic field B is $\varepsilon_\sigma = \varepsilon_0 - \sigma \mu_B B + U n_{\bar{\sigma}}$. The magnetic susceptibility of the impurity is derived from

$$\chi = -\mu_B^2 \sum_{\sigma} \frac{d\langle n_{\sigma} \rangle}{d\varepsilon_{\sigma}} \frac{1 - U \frac{d\langle n_{\sigma} \rangle}{d\varepsilon_{\sigma}}}{1 - U^2 \frac{d\langle n_{\bar{\sigma}} \rangle}{d\varepsilon_{\bar{\sigma}}} \frac{d\langle n_{\sigma} \rangle}{d\varepsilon_{\sigma}}}. \quad (29)$$

Figure 5 shows the occupation of the impurity spin level and the magnetic susceptibility as a function of y for the different inter-layer coupling in a bilayer graphene. The occupation $\langle n_{\sigma} \rangle$ versus y is a bubble that corresponds to the impurity magnetization. The corresponding susceptibility exhibits two peaks at the magnetization edge indicating the strength of the magnetic transition. For $t_p = 0$, a strong magnetic moment of $\sim 0.7\mu_B$ forms in almost the whole magnetic region. With increasing the inter-layer coupling t_p , the magnetic bubble region diminishes, signaling the decrease of the magnetic moment of the impurity, and the magnetic transition becomes very sharp. There is no localized magnetic moment in the case of a sufficiently strong inter-layer coupling. In this case, the magnetic boundary shrinks below the line $x = 6$ in the x direction (see figure 2(b)). Figure 6 shows the occupation of the impurity level and the magnetic susceptibility as a function of y for the different impurity energy level ε_0 in the bilayer graphene. The corresponding magnetic boundaries are defined in figures 3(a) and (b) respectively. For $V = 0$, the magnetic bubble shifts towards the $\langle n_{\sigma} \rangle$ axis, and decreases with increasing ε_0 . When ε_0 becomes large enough, the bubble

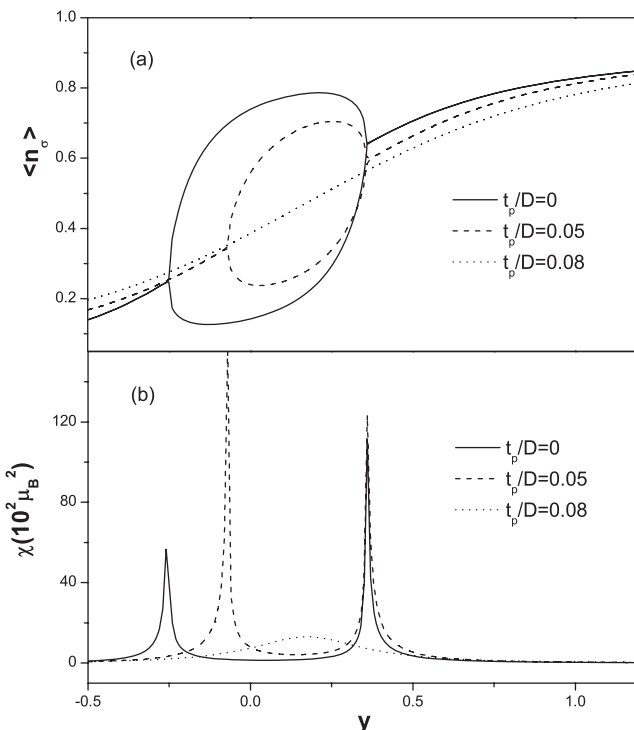


Figure 5. The occupation of the impurity spin level and the magnetic susceptibility in the bilayer graphene for the different t_p/D at $x = 6$. The other parameters are those of figure 2(b).

vanishes, meaning that the impurity loses magnetism in this situation. For large ε_0 the magnetic transition becomes very sharp. Inspecting figures 6(c) and (d), we find that when the gate bias V is applied the magnetic bubble shows a non-monotonic dependence on ε_0 , while the magnetic transition

becomes very sharp with increasing ε_0 . Since the magnetic boundary line shrinks on the left-hand side of the line $x = 4.2$ at $\varepsilon_0/D = 0.082$ (see figure 3(b)), the impurity remains non-magnetic for any y , i.e. $n_\uparrow = n_\downarrow$, as shown in figure 6(c).

5. Conclusions

Summarizing, we studied the localized magnetic states of an impurity in biased bilayer and trilayer graphene. We found that the size of the magnetic region decreases rapidly compared with that of a monolayer graphene. The impurity can magnetize even when the energy of the doubly occupied state is below the Fermi level and the impurity magnetization region has a different shape. We can trace this behavior back to the special nature of quasiparticles. When a gate bias is applied, the dependence of the impurity magnetic states on the impurity energy for the bilayer graphene shows a behavior different from that for a trilayer graphene due to the opening of a gap between the valence and the conduction band in the bilayer graphene. Correspondingly, the magnetic moment of the impurity versus the impurity energy in the bilayer graphene is affected strongly by the band gap induced by the gate bias.

Acknowledgments

The work of KHD was supported by the Natural Science Foundation of Hunan Province, China (grant No. 08JJ4002), the National Natural Science Foundation of China (grant No. 60771059), and the Education Department of Hunan Province, China. JB and ZHZ were supported by the cluster of excellence ‘Nanostructured Materials’ of the state Saxony-Anhalt.

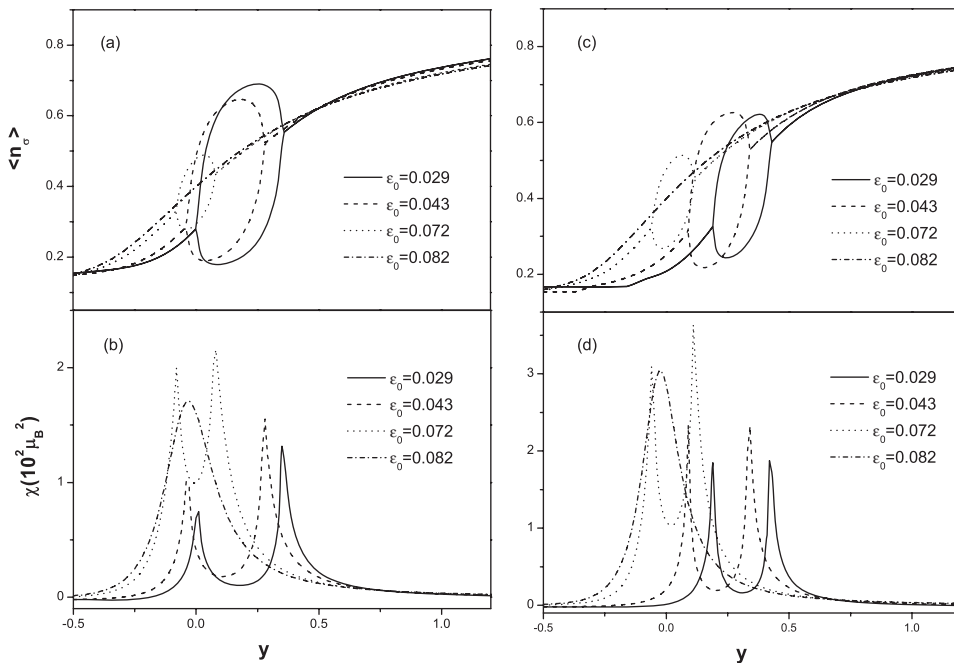


Figure 6. The occupation of the impurity spin level and the magnetic susceptibility in the bilayer graphene for different ε_0/D at $V/D = 0$ and $x = 3.2$ (a)–(b), and at $V/D = 0.05$ and $x = 4.2$ (c)–(d). The other parameters are the same as in figure 3.

References

[1] Novoselov K S, Geim A K, Morozov S V, Jiang D, Katsnelson M I, Grigorieva I V, Dubonos S V and Firsov A A 2005 *Nature* **438** 197

[2] Zhang Y, Tan Y W, Stormer H L and Kim P 2005 *Nature* **438** 201

[3] Geim A K and Novoselov K S 2007 *Nat. Mater.* **6** 183

[4] Castro Neto A H, Guinea F, Peres N M R, Novoselov K S and Geim A K 2009 *Rev. Mod. Phys.* **81** 109

[5] Novoselov K S, Geim A K, Morozov S V, Jiang D, Zhang Y, Dubonos S V, Grigorieva I V and Firsov A A 2004 *Science* **306** 666

[6] Berger C, Song Z, Li X, Wu X, Brown N, Naud C, Mayou D, Li T, Hass J, Marchenkov A N, Conrad E H, First P N and de Heer W A 2006 *Science* **312** 1191

[7] Huertas-Hernando D, Guinea F and Brataas A 2006 *Phys. Rev. B* **74** 155426

[8] Kane C L and Mele E J 2005 *Phys. Rev. Lett.* **95** 226801

[9] Yao Y, Ye F, Qi X L, Zhang S C and Fang Z 2007 *Phys. Rev. B* **75** 041401(R)

[10] Ding K H, Zhou G, Zhu Z G and Berakdar J 2008 *J. Phys.: Condens. Matter* **20** 345228

[11] Ding K H, Zhu Z G and Berakdar J 2008 arXiv:0811.3489

[12] Ponomarenko L A, Schedin F, Katsnelson M I, Yang R, Hill E H, Novoselov K S and Geim A K 2008 *Science* **320** 356

[13] Pedersen T G, Flindt C, Pedersen J, Mortensen N A, Jauho A P and Pedersen K 2008 *Phys. Rev. Lett.* **100** 136804

[14] Novoselov K S, McCann E, Morozov S V, Falko V I, Katsnelson M I, Zeitler U, Jiang D, Schedin F and Geim A K 2006 *Nat. Phys.* **2** 177

[15] Castro Eduardo V, Novoselov K S, Morozov S V, Peres N M R, Lopes dos Santos J M B, Nilsson J, Guinea F, Geim A K and Castro Neto A H 2007 *Phys. Rev. Lett.* **99** 216802

[16] Castro Eduardo V, Peres N M R, Stauber T and Silva N A P 2008 *Phys. Rev. Lett.* **100** 186803

[17] Han M Y, özyilmaz B, Zhang Y and Kim P 2007 *Phys. Rev. Lett.* **98** 206805

[18] Wimmer M, Adagideli I, Berber S, Tomanek D and Richter K 2008 *Phys. Rev. Lett.* **100** 177207

[19] Wang X, Ouyang Y, Li X, Wang H, Guo J and Dai H 2008 arXiv:0803.3464

[20] Guo J, Yoon Y and Ouyang Y 2007 *Nano Lett.* **7** 1935

[21] Zhang Y *et al* 2008 *Nat. Phys.* **4** 627
Geringer V *et al* 2009 *Phys. Rev. Lett.* **102** 076102 and references therein

[22] Duffy D M and Blackman J A 1998 *Phys. Rev. B* **58** 7443

[23] Uchoa B, Kotov V N, Peres N M R and Castro Neto A H 2008 *Phys. Rev. Lett.* **101** 026805

[24] Castro E V *et al* 2008 arXiv:0807.3348v1

[25] Nilsson J and Castro Neto A H 2007 *Phys. Rev. Lett.* **98** 126801

[26] Bostwick A *et al* 2007 *New J. Phys.* **9** 385
Ohta T *et al* 2006 *Science* **313** 951–4
Rotenberg E *et al* 2008 *Nat. Mater.* **7** 258–9 and references therein